Progress In Electromagnetics Research, Vol. 118, 71–87, 2011

FREQUENCY DOMAIN DYNAMIC THERMAL ANALYSIS IN GAAS HBT FOR POWER AMPLIFIER APPLICATIONS

T. T. Thein*, **C. L. Law, and K. Fu**

Positioning and Wireless Technology Center, 50 Nanyang Drive, Research TechnoPlaza, Nanyang Technological University, 637553, Singapore

Abstract—Dynamic temperature distributions in GaAs HBT are numerically analyzed in frequency domain as a function of power dissipation, frequency and space. Complete thermal characteristics, including frequency-dependent thermal impedance and phase lag behavior, are presented. The analysis is also extended for arbitrary periodic or aperiodic pulse heating operation to predict junction temperature of a Power Amplifier (PA) with non-constant envelope input signal. Dynamic junction temperatures of a single finger $2\,\mu\text{m} \times 20\,\mu\text{m}$ GaAs HBT are predicted for square pulse envelope signal input with power levels varying with up to 10 dB above a nominal average level of 40 mW and with pulse widths ranging from 10 ns to 100 µs. With the input envelope signal amplitude of 10 dB above the average, the analytical results show that junction temperature rises from room temperature of 27°C to 39°C when heated by 10 ns pulse and increases to 63°C by 100 ns pulse, 105°C by 1 µs pulse and to 198°C by 100 µs pulse. A novel setup is developed for nano-second pulsed measurements, and the analysis is validated through time domain on wafer pulsed measurements at three different power levels: 0 dB, 3 dB, and 6 dB above the average level. Results show that analytical results track well with measured junction temperature within the accuracy of ±5°C over the entire measurement set.

1. INTRODUCTION

Thermal effect plays an important role in RF and microwave power amplifiers (PA) where transistors are scaled into sub-micron size

Received 3 May 2011, Accepted 10 June 2011, Scheduled 24 June 2011

* Corresponding author: Than Tun Thein (N060107@e.ntu.edu.sg).

geometry and operated with high current densities. The temperature of the transistor depends on the heat generated inside it. The device reliability and both DC and RF performances of a PA are significantly degraded by the self heated transistor junction temperature (T_j). Self heating effect is extensively analyzed in the past and commonly included in standard bipolar compact models such as VBIC, HiCUM, MEXTRAM, and Agilent HBT [1–3]. First order equivalent thermal circuit with low pass behavior is used to predict T_j. Mutual heating between fingers of a power HBT is also analyzed and modeled as a thermal resistance matrix [4]. These models gave good results in predicting steady state thermal effects. However, they have limitation in predicting dynamic T_j. In general, four methods: (i) Numerical Analysis [5–7], (ii) 3D Simulation [8–10], (iii) Measurement [11], and (iv) Behavior Modeling [12–14], have been used to predict dynamic T_j for various applications. Among these, frequency-dependent dynamic T_j analysis is conducted using different envelope frequencies of up to 100 kHz in [11], 1 MHz in [10], and up to 10 MHz in [5, 9]. [10] reports that the thermal transient cutoff frequency is around 1 MHz, while [9] reported transient cutoff frequency of up to 10 MHz. These large variations in cutoff frequencies are due to the amount of heat dissipation and their dynamic variations in each case. For low power applications, small signal transient thermal analysis [15] is valid. However in the case of multi fingers power HBT and PA applications with large dynamic envelope amplitude variations above the average value, the use of small signal transient thermal analysis will produce erroneous results. The large dynamic envelope amplitude even for very short time durations, which are much smaller than the junction thermal time constant [8], may cause large dynamic fluctuations in junction temperature T_j.

Modern high speed communication systems use spectral efficient multi-carrier technique as Orthogonal Frequency Division Multiplexing (OFDM) and transmission efficiency improvement technique as Quadrature Amplitude Modulation (QAM). Regardless of individual carrier's characteristics, OFDM typically introduces peak to average power ratio (PAPR) of (8 to 13) dB, and QAM contributes another (3 to 6) dB [16]. Very high peaks generated from these systems can cause significant T_j excursion from the average, hence resulting in nonlinear current gain that highly depends on the magnitude of the adjacent symbol envelope. These nonlinear effects with memory cause distortion of the envelope resulting in data reception error and spill-over of signal into adjacent channels. These distortions are regulated in transmitter performance measures. Less than 3% error vector magnitude (EVM) is demanded in WiMAX [17]. There is a need for compact simulation

model that is able to model the short time dynamic thermal effect especially for the simulation and optimization of PA operating in high PAPR signals. In these PA, the collector (drain) supply is modulated at envelope frequency, and huge power fluctuation could occur in a short period of time. The signal envelope is complex and the dissipated power waveform contains various baseband components below the thermal cutoff frequency. The interaction of nonlinearity and dynamic effects makes T_j prediction and thermal modeling complex.

This leads us to analyze dynamic temperature behavior under CW, periodic arbitrary and aperiodic arbitrary pulse signal with high power. The interest includes very short time period of a few tens of nano-seconds, which need very fine mesh for finite element method (FEM) as 3D simulation, and this make it time consuming [18]. In this paper, temperature distributions in GaAs HBT are numerically analyzed in frequency domain, as a function of power dissipation, frequency and space. It incorporates frequency-dependent complex thermal impedance behavior in the transistor. Through the use of Fourier signal analysis, this thermal analysis is extended into arbitrary periodic or aperiodic pulse heating operation. To mimic the heating by multi-carrier signals which have tens of MHz bandwidth with high peak to average power ratio (PAPR), T_j for high power square pulses with power levels of 0 dB, 3 dB, 6 dB and 10 dB above the nominal average level of 40 mW and with pulse widths ranging from 10 ns to 100 μs, are analyzed. With the input square pulse signal amplitude of 10 dB above the average, the junction temperature is predicted to reach 39°C when heated by 10 ns pulse, increasing to 63°C by 100 ns pulse, 105°C by 1 μs pulse and to 198°C by 100 μs pulse. Time domain on wafer pulsed measurements of a single finger 2 μm × 20 μm GaAs HBT are conducted to validate the analysis. T_j increases as the pulse power and pulse width increase, and the comparison between analytical result and measurements of T_j for a 2 μm × 20 μm single finger GaAs HBT shows agreement within ±5°C over the entire measurement set.

2. NUMERICAL ANALYSIS

Heat is generated in the transistor by dissipated power and conducted through the substrate. It is very common in a transistor that the length of the active heat source is longer than all other dimensions, and it can be treated as a line source. The rectangular shape heat generating volume is transformed into an equivalent cylindrical volume and analyzed in cylindrical coordinates as heat is conducted in radial direction. Applying cylindrical coordinate simplifies two rectangular space variables, x and y, into a single radial variable r. Fig. 1 shows

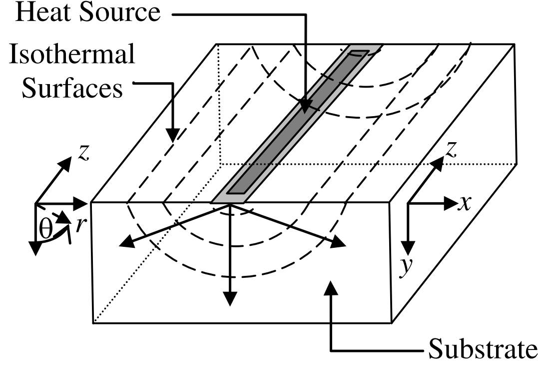

Figure 1. Single finger transistor schematic (un-scaled) with cylindrical isothermal surface.

the un-scaled geometry of a single finger HBT on the substrate with cylindrical isothermal surfaces. The initial and boundary conditions are assumed to be independent of θ and z coordinates along with the transistor, and the substrate is homogeneous and isotropic. The heat conduction equation in cylindrical coordinate with the presence of heat source is given by [19],

$$\frac{\partial^2 T_1}{\partial r^2} + \frac{1}{r}\frac{\partial T_1}{\partial r} + \frac{Q_0}{\kappa} = \frac{1}{\alpha}\frac{\partial T_1}{\partial t} \quad 0 \le r \le a \tag{1}$$

and the equation for the substrate without the heat source is,

$$\frac{\partial^2 T_2}{\partial r^2} + \frac{1}{r}\frac{\partial T_2}{\partial r} = \frac{1}{\alpha}\frac{\partial T_2}{\partial t} \quad a < r \le b \tag{2}$$

where: $T_r\,(r = 1, 2)$ is the temperature increment above the ambient temperature; Q_0 is heat flow rate per unit volume; κ is thermal conductivity of the material; α is the thermal diffusivity. The heat flow rate and thermal diffusivity can be expressed as: $Q_0 = P_0/(\pi r^2 L)$ and $\alpha = \kappa/\rho c$ respectively. Where: P_0 is power dissipation in the transistor; L is the length of the heat source; ρ is volumetric density; c is specific heat capacity of the substrate. Equations (1) and (2) are needed to satisfy initial and boundary conditions simultaneously.

2.1. Sinusoidal Thermal Wave

We first seek to analyze the dynamic thermal frequency response of (1) & (2), with the solution form as in [19],

$$T(t, r) = T_r(r)T_t(t) = T_r(r)e^{i\omega t} \tag{3}$$

Pure AC thermal sources (having negative heat power dissipation) cannot exist in reality. However, the frequency response can be measured experimentally [7]. By substituting (3) into (1) and (2), it follows that $T_r(r)$ must satisfy,

$$\frac{\partial^2 T_{r1}(\omega,r)}{\partial r^2}+\frac{1}{r}\frac{\partial T_{r1}(\omega,r)}{\partial r}-q^2T_{r1}(\omega,r) = -\frac{Q_0}{\kappa} \tag{4}$$

$$\frac{\partial^2 T_{r2}(\omega,r)}{\partial r^2}+\frac{1}{r}\frac{\partial T_{r2}(\omega,r)}{\partial r}-q^2T_{r2}(\omega,r) = 0 \tag{5}$$

with, $q^2 = i\omega/\alpha$. Equations (4) and (5) are non-homogeneous and homogeneous modified Bessel functions, respectively. Their general solutions can be written in the forms

$$T_{r1}(\omega,r) = T_{r1P}+C_1I(qr)+C_2K(qr) \tag{6}$$

$$T_{r2}(\omega,r) = C_3I(qr)+C_4K(qr) \tag{7}$$

where, T_{r1P} is the particular solution of $T_{r1}(\omega,r)$, and $I(qr)$ and $K(qr)$ are the first and second kinds of modified Bessel solutions. Four constant terms, $C_{1,2,3,4}$, have to be defined by using the following boundaries conditions,

$$\begin{aligned} &T_{r1}=\text{finite} \quad \text{at} \quad r=0, \quad T_{r2}=0 \quad \text{at} \quad r=b, \\ &T_{r1}=T_{r2} \quad \text{at} \quad r=a, \quad \frac{dT_{r1}}{dr}=\frac{dT_{r2}}{dr} \quad \text{at} \quad r=a, \end{aligned} \tag{8}$$

where, a is the volume equivalent radius of the heat source, and b is the thickness of substrate. Perfect cooling at $r = b$ is assumed and maintained at room temperature ($T_{amb} = 27^{\circ}$C). With the given boundaries conditions in Equation (8), the four coefficients are derived as,

$$C_1 = -\frac{Q_0a}{kq}\left[\frac{I_1(qa)}{I_0(qb)}K_0(qb)+K_1(qa)\right], \quad C_2=0 \tag{9}$$

$$C_3 = -\frac{Q_0a}{kq}\left[\frac{I_1(qa)}{I_0(qb)}K_0(qb)\right], \quad C_4=\frac{Q_0a}{kq}I_1(qa) \tag{10}$$

Substituting (9) and (10) into (6) and (7) gives the dynamic thermal behavior directly in the frequency domain as a function of power dissipation, frequencies and radial distance r. This scheme avoids the risk of unstable solutions associated with time domain and provides a complete, systematic dynamic characterization of the system [20].

A cylindrical heat source, which is volumetrically equivalent to a real single finger $2\,\mu$m $\times$ $2\,\mu$m HBT is analyzed. The considered schematic is shown in Fig. 1. GaAs is chosen as substrate material with the following thermal properties: $\kappa = 55\,\text{W/m}^{\circ}\text{C}$, $c = 330\,\text{J/kg}^{\circ}\text{C}$, and

$\rho = 5318\,\mathrm{kg/m^3}$. The thicknesses of the transistor and substrate are $1\,\mu\mathrm{m}$ and $75\,\mu\mathrm{m}$, respectively. A reference power level (40 mW) is set at half of the maximum current, 11 mA with 3.6 V power supply. The HBT is assumed to be driven by input signal at reference power level and then increases the dissipated power by 2 times, 4 times and 10 times compared to reference. (We will refer these power levels as 0 dB, 3 dB, 6 dB, and 10 dB respectively). For each chosen frequency and power level, T_j is computed numerically, using the aforementioned analysis.

The calculated T_j as a function of frequency is plotted in Fig. 2. The results show that as the frequency (f) increases from 10 kHz to 30 MHz at fixed power dissipation, T_j drops linearly with log (f). It is also noted that T_j rises from 48°C to 262°C for 10 kHz input signal at 10 dB power overdrive. However, if the input signal frequency increases to 30 MHz at the same power overdrive, T_j increases from 27°C to 54°C. These results show that there will be significant dynamic T_j changes in a transistor when non constant envelope signal with high PAPR is present at the input. Fig. 3 shows the temperature distribution along the radial direction into the substrate. As the generated heat spread out to the wider substrate, the temperature field is attenuated and decays exponentially with distance from the junction. The decay rate increases with frequency and is often characterized by a parameter known as thermal layer thickness (δ) [21], beyond which the substrate temperature remains unchanged. As thermal impedance (Z_{th}) varies with heated volume, this indicates significant thermal

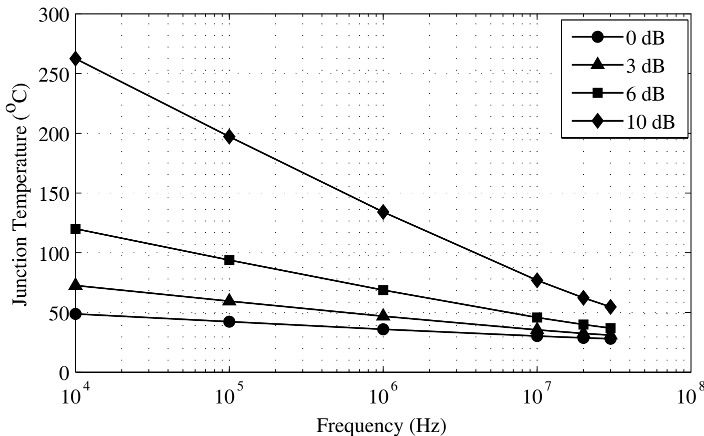

Figure 2. Frequency-dependent junction temperature (T_j) at different power levels.

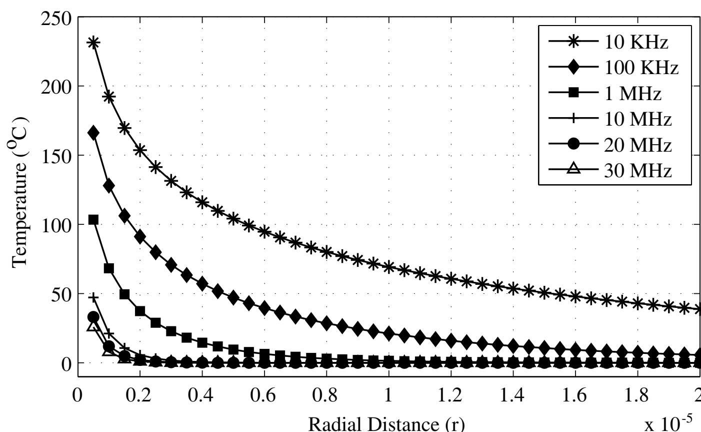

Figure 3. Frequency-dependent Temperature distribution into the substrate, power = 10 dB.

impedance changes at higher frequencies. Moreover, as heat cannot be transferred at infinite speed [19], it takes significant time lag for the temperature at a particular radial distance to follow the instantaneous power dissipation in the transistor. This frequency-dependent delay introduces certain amount of phase lag,

$$T_r(\omega, r) = |T_r|\, e^{j\Phi_1(\omega,r)} \tag{11}$$

This phase lag parameter is an important factor for multiple sinusoidal thermal waves such as those encountered in dynamic T_j analysis under pulse heating conditions. The various frequency components of the pulse will have different phases lag with respect to each other and hence may introduce constructive or destructive effects on the resultant thermal fields at a particular radial distance. However, the phase does not change with power. Fig. 4 shows the computed phase lag at the junction radial distance, $r = a$ at different frequencies. The ac thermal impedance can be defined as the temperature rise ΔT in a volume for a unit quantity of heat supplied ΔQ,

$$Z_{th}(\omega, r) = \frac{\Delta T_r(\omega, r)}{\Delta Q} \tag{12}$$

Figure 5 shows the ac thermal impedance Z_{th} which is complex frequency dependent parameter at the junction radial distance $r = a$. Frequency-dependent nonlinear thermal impedance is clearly observed. This correlates well with thermal impedance analyzed by [7, 22]. In reality, Z_{th} varies with power through temperature-dependent thermal

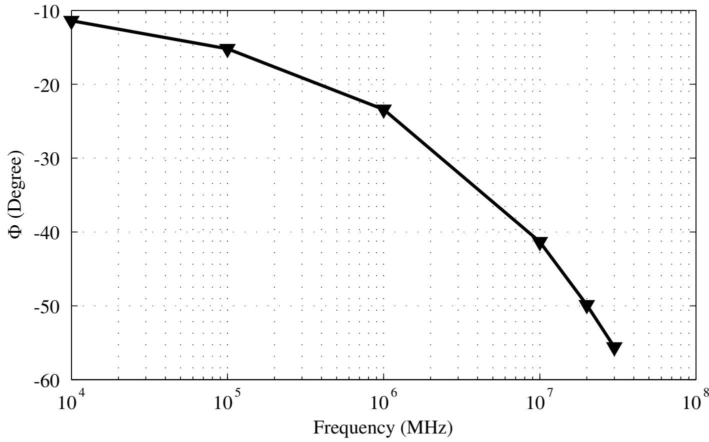

Figure 4. Frequency-dependent phase lagging of thermal wave in GaAs, $r = a$.

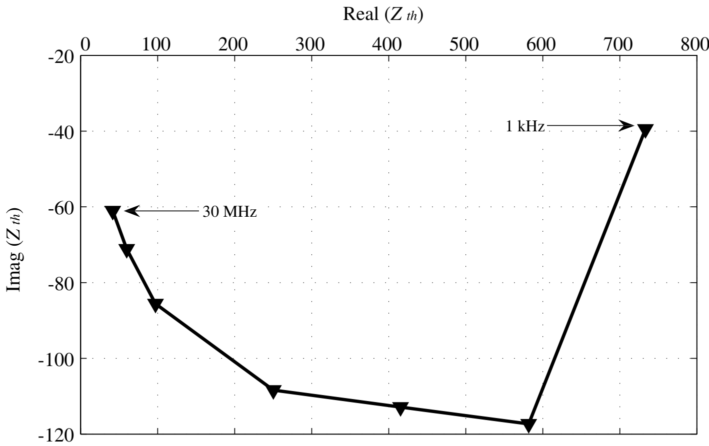

Figure 5. Frequency-dependent nonlinear thermal impedance of the transistor.

conductance. However, isotropic assumption in this analysis makes Z_{th} as power independent.

2.2. Periodic and Aperiodic Arbitrary Wave

In the case of non-constant envelope signal input, the resultant power wave $P_0(t)$ contains various baseband components below the thermal

cutoff frequency. The frequency-dependent thermal wave Equations (6) and (7) can be used to analyze the resultant thermal field. Using Fourier analysis, the amplitude and phase spectrum of $P_0(t)$ can be evaluated as,

$$\begin{aligned} P_0(\omega) &= \sum_{n=-\infty}^{n=\infty} c_n = \sum_{n=-\infty}^{n=\infty} |c_n| e^{j\Phi_n(\omega)} \\ &= \sum_{n=-\infty}^{n=\infty} \frac{1}{T_0} \int_{-\tau/2}^{\tau/2} P_0(t) e^{-j2\pi n \Delta f t} dt \end{aligned} \quad (13)$$

By substituting Equation (13) into Equations (6) and (7), the dynamic temperature response to arbitrary shape periodic power waveform heating can be evaluated. The total phase shift at a particular frequency shown in Equation (11) becomes,

$$T_r(\omega, r) = |T_r|\, e^{j\Phi(\omega,r)} = |T_r|\, e^{j\Phi_1(\omega,r)+\Phi_n(\omega)} \quad (14)$$

By setting $\lim \Delta f \longrightarrow 0$, Equation (13) can be adopted for arbitrary shape aperiodic signal. So, this analysis is applicable to a wide range of signal types, from CW to arbitrary pulse, at different power levels, various substrate positions and material properties.

2.3. Square Pulse Signal

Dynamic thermal response to square pulses signal input to the transistor is analyzed. Pulse widths (τ), ranging from 10 ns to 100 µs

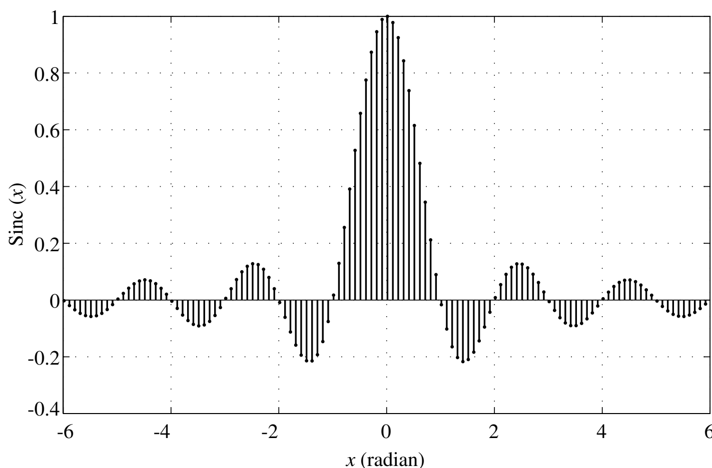

Figure 6. Normalized and truncated fourier coefficients of a square pulse.

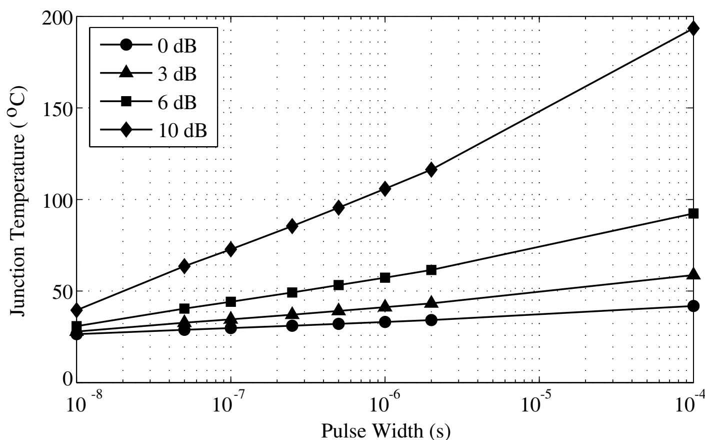

Figure 7. Predicted junction temperature for various pulses widths at different power levels.

with pulse repetition rate (PRF) of 1 kHz, are selected to be analyzed at various power levels. Isolating the steady state heating effect, the analysis is conducted with no average power level. The amplitude and phase of each frequency component of the pulse signal are determined using (13). Fig. 6 shows the normalized amplitude and phase spectrum of c_n in a single graph. Fourier coefficients, c_n, of the square pulse are real, and consequently, the phase spectrum is either zero, when c_n is positive, or π when c_n is negative. $T_r(\omega, r)$ is then calculated at every frequency component within a truncated range. The temperature contributed from each frequency component is summed up in a vector form. Fig. 7 shows the computed T_j as a function of pulse width and power. The results show that as pulse power increases from 0 dB to 10 dB, T_j is raised to 40°C for 10 ns pulse, 72°C for 100 ns pulse, 105°C for 1 µs and to 193°C by 100 µs.

3. INVESTIGATION THROUGH MEASUREMENTS

3.1. Measurement Setup

To validate the analysis, time domain on wafer measurement is carried out using a single finger 2 µm × 20 µm InGaP/GaAs HBT. We introduce a novel measurement setup where both pulsed base and collector can be applied. Matched load conditions with DC signal coupling are provided at both the base and collector monitoring circuits for measurements with a wide range of pulse width from DC to a few ns.

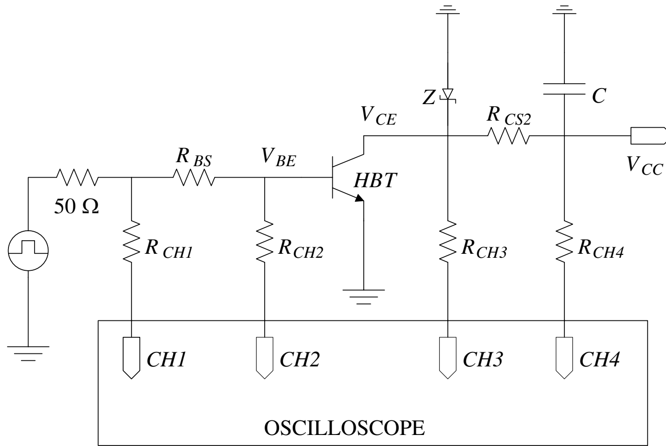

Figure 8. Time domain pulsed thermal measurement setup.

The measurement setup is shown in Fig. 8. A base current sensing resistor (R_{BS}) is inserted in series between the pulse generator and the base of the transistor. The voltages across R_{BS} are measured through sensing resistors R_{CH1} and R_{CH2}. Precise indication of I_b and V_{be} is mandatory in these measurements. The values of R_{BS}, R_{CH1} and R_{CH2} are optimized for a given range of I_b and V_{be}. In these measurements, I_b is in the range of 10 µA to 10 mA, while V_{be} is ranging from 1.3 V to 1.6 V. The values used are $R_{BS} = 500\,\Omega$, $R_{CH1} = 1\,\mathrm{k}\Omega$, and $R_{CH2} = 1\,\mathrm{k}\Omega$. Similarly, R_{CS} is used to sense the collector current by the measurement of potential difference across it through sensing resistors R_{CH3} and R_{CH4}. The value of R_{CS} should be chosen to ensure that the HBT is in a stable condition in addition to consideration of I_c measurement accuracy. In these measurements, I_c is in the range of 1 mA to 200 mA. The values used are $R_{CS} = 50\,\Omega$, $R_{CH3} = 1\,\mathrm{k}\Omega$, and $R_{CH4} = 1\,\mathrm{k}\Omega$. DC feed inductor is eliminated to minimize voltage spike [23]. A shunt capacitor C is added to provide instantaneous charges at the rising edges. A zener diode is added in shunt to prevent the HBT from damage during off period. All sampled voltages at the oscilloscope are de-embedded to the base and collector of the HBT. 50 Ω cables are used to connect the voltage monitoring points to the oscilloscope, and the input impedance of the oscilloscope is set to 50 Ω to prevent reflections. A sample measured time domain pulse response, de-embedded to base and collector, for 10 ns input with constant V_{cc} is shown in Fig. 9. The HBT is biased in the common emitter configuration for Class-C operation. It has a cutoff frequency of 35 GHz, a maximum frequency of oscillation of more than 100 GHz,

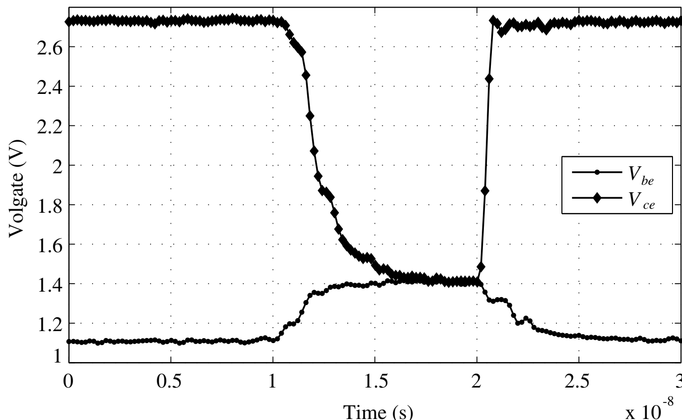

Figure 9. Measured time domain pulse response for 10 ns input with constant V_{cc}.

a common base open-emitter break down voltage (BVCBO) of 30 V, a common emitter open-base breakdown voltage (BVCEO) of 16 V and a common emitter open-collector breakdown voltage (BVBEO) of 7 V.

3.2. Thermal-Dependent V_{be} Characterization

First, we characterize the dependency of V_{be} on temperature. V_{be} variation with temperature is measured at fixed I_b by using a Semiconductor Parameter Analyzer (SPA). The base plate temperature of the HBT is varied from 25°C to 120°C using a heated platform, and V_{ce} is varied from 1 V to 4.5 V with 0.5 V step. Fig. 10 shows measured V_{be} at different power dissipations. Results show that V_{be} reduces as base plate temperature and power dissipation increases. It is also noted that V_{be} is a nonlinear function of power, and it drops linearly with temperature at around 1.3 mV/°C as shown in Fig. 11.

3.3. Result and Discussion

The input pulse widths ranging from 10 ns to 100 µs are selected for this identification to cater for wide range of signal bandwidth. To eliminate heat accumulation effect, PRF of 10 Hz is set to 100 µs pulse, and 1 kHz is set for the rest. The pulses are superimposed on 1.1 V DC generated from a HP8131A pulse generator and applied to the base. A DC power supply is directly connected to V_{cc} and adjusted so that $V_{be} = V_{ce}$ ($V_{bc} = 0$) is maintained for all pulse amplitudes. This ensures that the power is solely dissipated in the Base-Emitter

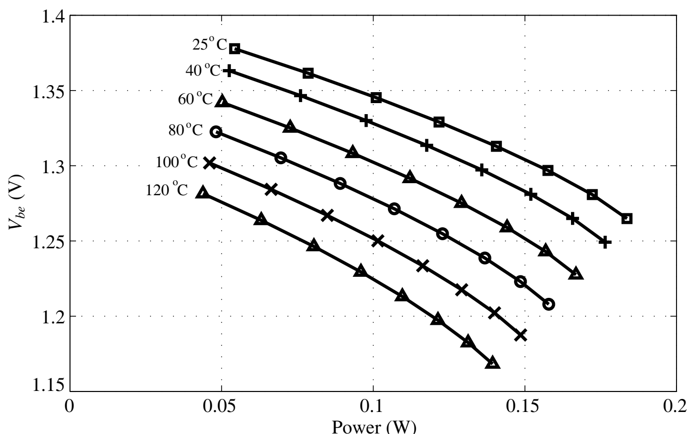

Figure 10. Measured V_{be} at different power levels, with various base plate temperatures.

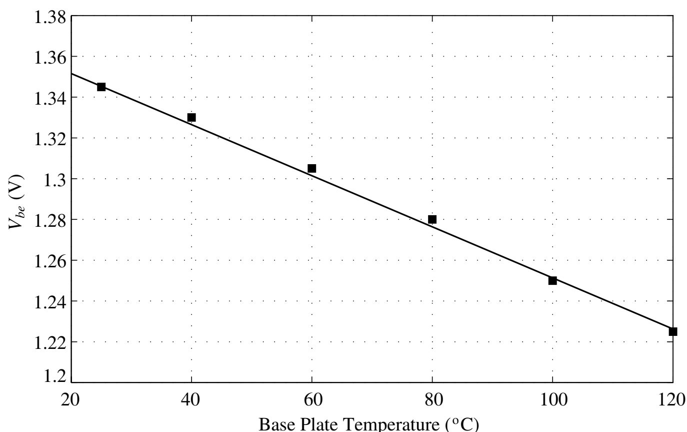

Figure 11. Measured V_{be} for different base plate temperature, power = 100 mW.

junction. Measurements are conducted at three different power levels: 0 dB, 3 dB and 6 dB above 40 mW.

However, due to the limitations in equipments power handling, 10 dB power level is dropped from the measurement. V_{be} are monitored for different input pulse widths and shown in Fig. 12. The corresponding collector current drop is shown in Fig. 13. Results show that V_{be} drops by 15 mV, 37 mV and 75 mV with increasing pulse

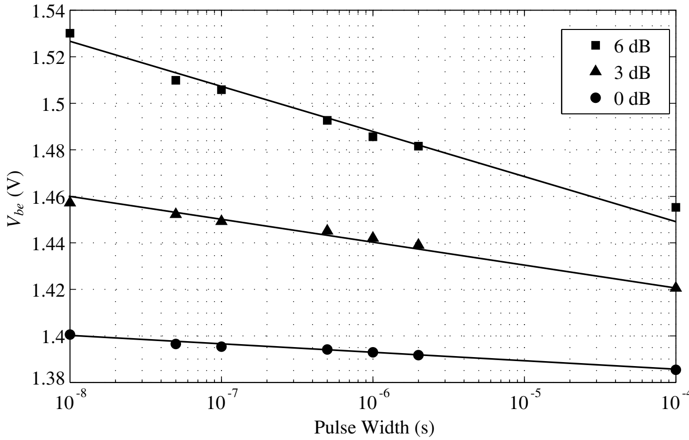

Figure 12. V_{be} variation under pulsed measurements, power levels.

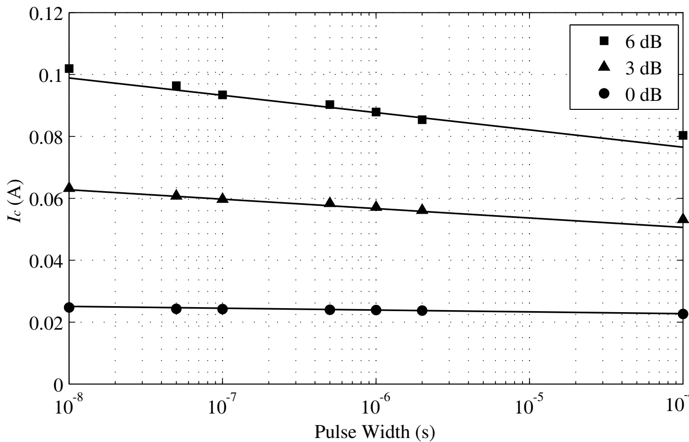

Figure 13. Corresponding I_c variation under pulsed measurements, power levels.

width from 10 ns to 100 µs, for 0 dB, 3 dB and 6 dB power levels, respectively. Meanwhile, the collector currents drop 2 mA, 10 mA and 21 mA accordingly. As shown in earlier analysis, 10 ns pulse with 0 dB power level is short enough to ensure that the transistor is not heated up and isothermal condition is set. The response of the transistor in this case can be assumed to be purely electrical. Hence, the base-emitter voltage corresponding to 10 ns pulse with 0 dB power level is taken as a reference. Assuming a V_{be} temperature dependent coefficient of 1.3 mV/°C, the junction temperature T_j is

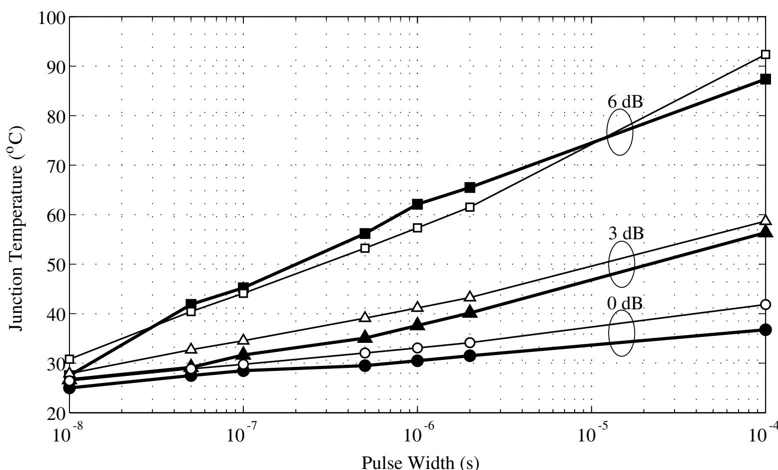

Figure 14. Junction temperature (T_j) measured (black symbol) verses analytically predicted (white symbol) at different power levels.

extracted from the measured data. Fig. 14 shows the extracted T_j from measurement and analytically predicted. Close agreements between measured and analytically predicted junction temperatures within ±5°C are observed.

4. CONCLUSIONS

Dynamic heating in GaAs HBT by high power pulse signal is analyzed in frequency domain. The analysis is applicable to a wide range of signal types, power levels, frequencies, substrate position and material properties. Short period excessive power heating effect is integrated into the analysis to accurately predict the junction temperature for Power Amplifier with non-constant envelope input signal. The integrated analysis is applied to predict the junction temperature for high power square pulses with a wide range of pulse width, including pulse width as short as 10 ns. Time domain on wafer pulsed measurement setup is developed for short pulse width measurements, and the accuracy of the pulsed thermal analysis is validated. ±5°C accuracy over entire measurement set is achieved.

ACKNOWLEDGMENT

This work was supported by the ASTAR project under the Grant 062-101-0029.

REFERENCES

1. Rudolph, M., *Introduction to Modeling HBTs*, Artech House, 2006.
2. Liu, W., *Handbook of III-V Heterojunction Bipolar Transistors*, Wiley-Interscience, New York, 1998.
3. Marsh, S. P., "Direct extraction technique to derive the junction temperature of HBT's under high self-heating bias conditions," *IEEE Trans. Electron. Devices*, Vol. 47, No. 2, 288–317, 2000.
4. Wenhua, D., P. Robin, and M. Frei, "Distributed and multiple time-constant electro-thermal modeling and its impact on ACPR in RF predistortion," *62nd ARFTG Microwave Measurements Conference*, NJ, USA, Dec. 2003.
5. Batty, W., et al., "Electrothermal CAD of power devices and circuits with fully physical time-dependent compact thermal modeling of complex nonlinear 3-D systems," *IEEE Trans. Compon. Packag. Technol.*, Vol. 24, No. 4, 566–590, 2001.
6. Clemente, S., "Transient thermal response of power semiconductors to short power pulses," *IEEE Trans. Power Electron.*, Vol. 8, No. 4, 337–341, 1993.
7. Vermeersch, B. and G. De Mey, "Influence of substrate thickness on thermal impedance of microelectronic structures," *Microelectron. Reliab.*, Vol. 47, No. 2, 437–443, 2007.
8. Baxter, G., "Transient temperature response of a power transistor," *IEEE Trans. Parts Hybrids Packag.*, Vol. 10, No. 2, 132–137, 1974.
9. Le Gallou, N., et al., "Analysis of low frequency memory and influence on solid state HPA intermodulation characteristics," *IEEE International Microwave Simposium*, 979–982, Phoenix, USA, 2001.
10. Takahashi, Y., R. Ishikawa, and K. Honjo, "Precise modeling of thermal memory effect for power amplifier using multi-stage thermal RC-ladder network," *Asia-Pacific Microwave Conference*, 287–290, Yokohama, Japan, 2006.
11. Sommet, R., et al., "On the determination of the thermal impedance of microwave bipolar transistors," *12th IEEE Intersociety Conference on Thermal and Thermomechanical Phenomena in Electronic Systems*, 1–8, Las Vegas, USA, 2010.
12. Mazeau, J., et al., "Behavioral thermal modeling for microwave power amplifier design," *IEEE Trans. Micro. Theory Tech.*, Vol. 55, No. 11, 2290–2297, 2007.

13. Camarchia, V., et al., "Self-consistent electrothermal modeling of class A, AB, and B power GaN HEMTs under modulated RF excitation," *IEEE Trans. Micro. Theory Tech.*, Vol. 55, No. 9, 1824–1831, 2007.
14. Melczarsky, I., et al., "Compact empirical modeling of nonlinear dynamic thermal effects in electron devices," *IEEE Trans. Micro. Theory Tech.*, Vol. 56, No. 9, 2017–2024, 2008.
15. Lonac, J. A., et al., "A simple technique for measuring the thermal impedance and the thermal resistance of HBTs," *Gallium Arsenide and Other Semiconductor Application Symposium*, 197–200, Paris, France, 2005.
16. Raab, F. H., et al., "Power amplifiers and transmitters for RF and microwave," *IEEE Trans. Micro. Theory Tech.*, Vol. 50, No. 3, 814–826, 2002.
17. IEEE802.16, "Transmitter constillation error and test method, in air interface for fixed and mobile broadband wireless access systems," *IEEE*, NY, USA, 2004.
18. Noijen, S. P. M. and H. J. Eggink., "Effective thermal modeling of discrete components under peak-pulsed power loading by subdomain consideration," *International Conference on Thermal, Mechanical and Multi-Physics Simulation and Experiments in Microelectronics and Micro-Systems*, 1–5, Freiburg-im-Breisgau, Germany, 2008.
19. Carslaw, H. S. and J. C. Jaeger, *Conduction of Heat in Solids*, Oxford University Press, USA, 1986.
20. Vermeersch, B. and G. De Mey, "A shortcut to inverse fourier transforms: Approximate reconstruction of transient heating curves from sparse frequency domain data," *Int. J. Therm. Sci.*, Vol. 49, No. 8, 1319–1332, 2010.
21. Kakac, S. and Y. Yener, *Heat Conduction*, Taylor & Francis, NY, USA, 1985.
22. Vermeersch, B. and G. De Mey, "Thermal impedance plots of micro-scaled devices," *Microelectron. Reliab.*, Vol. 46, No. 1, 174–177, 2006.
23. Xia, J., C. L. Law, and T. T. Thein, "Generation of sub-nanosecond 7 V Gaussian pulse using GaAs HBT with 3 V battery supply," *Asia-Pacific Microwave Conference*, 1605–1608, Singapore, Singapore, 2009.